Synthetic Metals 199 (2015) 292–302

Contents lists available at ScienceDirect

Synthetic Metals

journal homepage: www.elsevier.com/locate/synmet

Magnetic composites of $CoFe_2O_4$ nanoparticles in a poly(aniline) matrix: Enhancement of remanence ratio and coercivity

P.S. Antonel [a], F.M. Berhó [a], G. Jorge [b], F.V. Molina [a,*]

[a] Instituto de Química Física de Materiales, Ambiente y Energía (INQUIMAE), Facultad de Ciencias Exactas y Naturales, Universidad de Buenos Aires, Ciudad Universitaria, Pabellon II, Piso 1, C1428EGA Buenos Aires, Argentina

[b] Instituto de Ciencias, Universidad Nacional de General Sarmiento, Juan M. Gutiérrez 1150 (B1613GSX), Los Polvorines, Provincia de Buenos Aires, Argentina

ARTICLE INFO

Article history:
Received 22 July 2014
Received in revised form 14 November 2014
Accepted 2 December 2014
Available online 9 December 2014

Keywords:
Nanostructures
Oxides
Magnetic properties

ABSTRACT

Magnetic composites of cobalt ferrite nanoparticles and poly(aniline) have been synthesized in acid media and characterized by X-ray diffraction studies, scanning and transmission electron microscopy observation, thermogravimetric analysis, conductivity and infrared spectroscopy measurements. The magnetic behavior was studied through DC magnetization measurements; hysteresis loops were observed, showing ferromagnetic behavior for particles and composites. The remanence ratio increases as the polymer contents increases, the coercivity decreases first and then increases, and the saturation magnetization does not follow the ferrite mass fraction in the composite. It is proposed that an indirect exchange mechanism (RKKY-like) between the nanoparticles and PANI localized spins mediated by the conduction electrons is responsible for the observed magnetic behavior. The results suggest the presence of particle–matrix interactions related to the amount of polymer present, thus, in turn suggesting that the material magnetic properties could be controlled through the nanoparticles to polymer ratio.

1. Introduction

Among the wide variety of nanomaterials which have been introduced in recent years, magnetic nanoparticles are highly interesting, due to their potential applications in different fields [1–3]. Whereas, larger particles are composed of several magnetic domains, below a certain (composition dependent) critical size, magnetic nanoparticles behave as monodomains, which give rise to interesting properties [1,4,5]. A number of materials have been investigated, mainly iron and iron oxides [6,7], ferrites [8,9] and other metals [10,11]; among these, cobalt ferrite ($CoFe_2O_4$) is highly interesting, since, it is a hard material from the magnetic point of view (exhibiting ferromagnetism at room temperature), has a high coercive field and moderate saturation magnetization and, in addition, displays excellent chemical stability [12].

In recent years, there has been a growing interest in composites formed by magnetic nanoparticles embedded in a polymer matrix [4,13,14], particularly of conducting polymers. Conducting polymers are very well known due to their interesting chemical, mechanical and optical properties leading to a high number of proposed applications [15–17]. A number of magnetic nanoparticle-conducting polymer composites have been proposed, mainly based on polypyrrole (PPy) [18,19], poly(ethylenedioxythiophene) [20] and poly(aniline) (PANI) [21–28]. The use of conducting polymers gives rise to materials with properties that would be difficult to obtain with the individual components, since, they have both high magnetic susceptibilities and high conductivity [29,30]. These magnetic composite materials comprise a new generation of multifunctional materials that combine the properties of ordinary polymer and magnetic materials (ferri- and/or ferromagnetic particles mixed or embedded in a matrix). Such materials have been proposed for several applications: Radhakrishnan et al. [31] synthesized PANI–Fe_3O_4 composites and showed its application as an electrochemical dopamine sensor and supercapacitor material; Bhaumik et al. [32] demonstrated the use of PPy–magnetite composites for fluoride adsorption and removal from water; Wuang et al. [33] obtained PPy–Fe_3O_4 nanoparticles functionalized with folic acid for cancer treatment; several authors have pointed out the electromagnetic shielding capability of composites such as PANI–γ-Fe_2O_3 [34], PANI–TiO_2–γ-Fe_2O_3 [35] or PANI–Fe_3O_4 [36]; PANI–cobalt ferrite composites have been reported to show high shielding efficiency [23]. All these applications underline the importance of the study of these materials from an applied point of view, besides the fundamental interest.

PANI is one of the most studied conducting polymers, due to its interesting properties and applications [15,37]. $CoFe_2O_4$–PANI

* Corresponding author. Tel.: +54 11 4576 3378; fax: +54 11 4576 3341.
E-mail addresses: sole@qi.fcen.uba.ar (P.S. Antonel), flaviamberho@hotmail.com (F.M. Berhó), gjorge@df.uba.ar (G. Jorge), fmolina@qi.fcen.uba.ar (F.V. Molina).

http://dx.doi.org/10.1016/j.synthmet.2014.12.003
0379-6779/

composites have not received much attention in the literature; there are some recent reports [23,38] which have synthesized the composite and measured its properties, however, little attention was given to the analysis of the magnetic behavior. Also, the possible effects of particle–matrix interactions on the composite properties are not well understood; for example, there are opposite reports about the influence of magnetic particles on the polymer conductivity, where some authors report an increase [39,40] whereas others show a decrease [33,41].

In this work, $CoFe_2O_4$–PANI composites have been prepared by a wet chemical method, with in situ aniline polymerization. The composites were characterized by XRD studies, SEM and TEM observation, thermogravimetric analysis, conductivity measurements, IR spectroscopy and DC magnetization measurements.

2. Materials and methods

AR grade chemicals and high purity water from a Milli-Q system were employed throughout. Aniline (Ani), supplied by Fluka, was distilled under reduced pressure and reducing conditions shortly before the experiments.

2.1. Synthesis of cobalt ferrite nanoparticles

The synthesis of $CoFe_2O_4$ nanoparticles was performed following Antonel et al. [14]. Briefly, 22.25 mL of a solution containing 0.450 M $FeCl_3{\cdot}6H_2O$ and 0.225 M $CoCl_2{\cdot}6H_2O$ (2:1 Fe(III)–Co(II) molar ratio), in 0.4 M HCl, was added dropwise to 200 mL of 1.5 M NaOH, keeping the pH adjusted at 12, under constant high speed stirring. The synthesis temperature was set at 80 °C, using a water-jacketed reaction vessel with a circulating thermostatic bath. Dark brown $CoFe_2O_4$ nanoparticles precipitated immediately after the first drops of the Fe(III)–Co(II) solution. The temperature of synthesis and the high speed stirring were kept constant during the addition of the cationic solution. After the addition of this solution, the reaction media was maintained at 80 °C, at high speed stirring, for 2 h. The $CoFe_2O_4$ nanoparticles were separated by centrifugation at 12,000 × *g* during 20 min at room temperature. The pellet was washed with Milli-Q water, repeating the cycles of washing–centrifugation until neutral pH of the supernatant was reached (about 10 times). Finally, the $CoFe_2O_4$ nanoparticles were dried using a vacuum oven at 40 °C during 24 h.

2.2. Synthesis of $CoFe_2O_4$–PANI composites

The synthesis of $CoFe_2O_4$–PANI composites was performed following Xuan et al. [42] with some modifications. 80 mg of $CoFe_2O_4$ nanoparticles and 400 mg of poly(vinylpyrrolidone) (PVP) were dispersed in 100 mL of Milli-Q water, by combined ultrasound treatment and under strong mechanical stirring, during 30 min, in order to disperse efficiently the particles, and to allow polymer adsorption onto the particles so as to protect them. Then, Ani monomer (in a given molar ratio, *r*, with respect to ferrite, see below) and 200 μL of concentrated HCl were added; next, the reaction mixture was maintained for 1 h in the same conditions (ultrasound treatment and strong mechanical stirring). Finally, ammonium persulfate (APS) in a molar ratio of 1:1 with respect to Ani was added. After APS addition, the reaction mixture was kept for 2 h always under ultrasound treatment and mechanical stirring. The dark green precipitate obtained was separated by centrifugation at 15,000 × *g*, during 10 min, at 17 °C. The pellet was repeatedly washed with Milli-Q water and ethanol, in order to remove the excess of reactants and oligomers (by-products of the polymerization reaction). Finally, the pellets were dried at room temperature for 24 h.

The synthesis was performed for different values of the molar ratio

$$r = \frac{n_{\mathrm{Ani}}}{n_{\mathrm{CoFe_2O_4}}} \quad (1)$$

where n_{Ani} and $n_{\mathrm{CoFe_2O_4}}$ are the mole numbers of Ani monomer and $CoFe_2O_4$, respectively. In the above specified conditions, *r* was varied between 5 and 20. For comparison purposes, PANI without ferrite particles was synthesized as above both in the presence (PANI–PVP) and in the absence (Pure PANI) of PVP; moreover a composite with $r = 5$, without PVP (no-PVP) was also synthesized.

2.3. Characterization of $CoFe_2O_4$ nanoparticles and $CoFe_2O_4$–PANI composites

2.3.1. X-ray diffraction (XRD)

X-ray powder diffraction analysis of the nanoparticles was performed with a Philips X-Pert diffractometer using Cu Kα radiation ($\lambda = 0.154056$ nm); the average crystallite size was determined with the Debye–Scherrer equation.

2.3.2. Electron microscopy studies

The particle size, morphology and composition of particles and composites were studied by transmission electron microscopy (TEM), scanning electron microscopy (SEM) and energy dispersive X-ray spectroscopy (EDS). TEM observation was performed using a transmission electron microscope Philips EM 301. Each material (nanoparticles or composites) was suspended in acetone and approximately 10 μL of each suspension were dripped on a TEM grid and dried prior to insertion to TEM column. SEM analysis was performed using a Zeiss Supra 40 Gemini microscope, equipped with an EDS detector. The samples were prepared by placing a small amount of each solid (nanoparticles or composites) in one side of a carbon tape. EDS measurements were performed in the same experiment.

2.3.3. Thermal analysis

Thermogravimetric analysis (TGA) of $CoFe_2O_4$ nanoparticles, $CoFe_2O_4$–PANI composites and PANI polymer was performed using a thermobalance TGA-51H Shimadzu. The TGA thermograms were recorded for 10–20 mg of each sample at a heating rate of 10° C/min in the temperature range of 25–800 °C under air atmosphere.

2.3.4. Fourier transform infrared spectroscopy (FTIR)

The infrared (IR) measurements of composites, nanoparticles and polymer were performed using a FTIR Nicolet 8700 spectrometer, in the range 400–4000 cm^{-1}. The samples were pressed into pellets prepared dispersing 0.5 mg of each one in 150 mg of KBr. For each sample, 32 scans were accumulated.

2.3.5. Conductivity measurements

The conductivity of the different samples was measured on pressed circular pellets (1 cm diameter) using a Teq-03 (S. Sobral, Buenos Aires, Argentina) potentiostat under computer control. Following Ohm's law, a known current (*i*) was applied and the potential difference (*E*) was measured and averaged during 120 s. The resistance was determined for each applied current and potential; the pellet thickness was measured with a caliper. The conductivity was determined for the as-obtained composites as well as for the same composited redoped by soaking in 1 M $HClO_4$ for 24 h, and drying in vacuum oven at 40 °C.

2.3.6. Magnetization studies

A Lakeshore 7400 vibrating sample magnetometer (VSM) was used for recording magnetization curves at room temperature. The

samples were prepared by packing with Teflon tape 10–20 mg of each composite.

3. Results and discussion

3.1. $CoFe_2O_4$ nanoparticles characterization

3.1.1. Crystalline structure and composition

The XRD pattern of the particles obtained is shown in Fig. 1, where a typical inverse spinel pattern is observed (ICDD 03-0864), very similar to that of Fe_3O_4 [8,43]. The diameter of the crystallites, d_c, prepared here was estimated through the Debye–Scherrer equation using the (3 1 1) peak, resulting in d_c = 16.5 nm which is in agreement with reported results [8,14]. The composition was verified from the SEM–EDS measurements, resulting in a Fe:Co molar ratio of 2:1, thus confirming that the product obtained was effectively $CoFe_2O_4$.

3.1.2. Particle size and morphology

The morphology of the cobalt ferrite particles was analyzed using SEM and TEM imaging. Fig. 2a shows a typical SEM image, where it is observed that the nanoparticles have an approximately spherical shape. Due to agglomeration, it is difficult to determine particle sizes on these images; TEM observation, on the other hand (Fig. 2b shows a typical TEM image), allows the particle diameters to be measured in the low agglomeration zones. Over 100 particles were measured in a set of images with the aid of the ImageJ software [44]; background subtraction and contrast enhancement were employed to improve particle detection and measurement. Care was exercised to discriminate agglomerates from single particles. The resulting histogram is shown in the inset of Fig. 2b, revealing a good monodispersity. The average particle diameter is $d_P = (17.3 \pm 1.0)$ nm, which is reasonably coincident with d_c determined from the Debye–Scherrer equation, thus it can be concluded that the cobalt ferrite particles obtained are single crystals. Furthermore, this size is within the range of monodomain magnetic particles: according to several authors [8,45], for cobalt ferrite, the minimum ferromagnetic size is about 7–9 nm; on the other hand, the critical particle size can be estimated, following O'Handley [46], as:

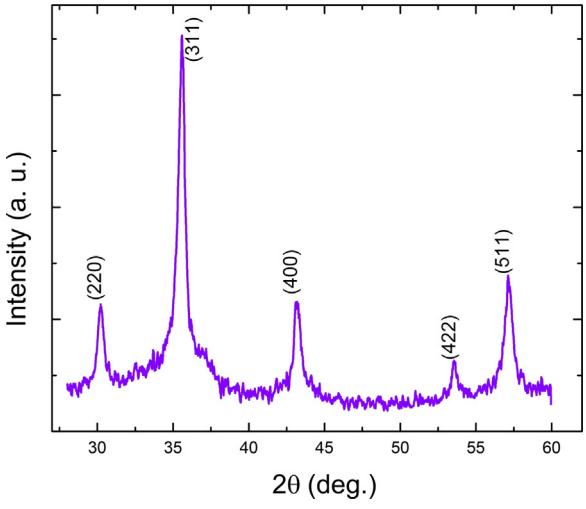

Fig. 1. XRD diagram of $CoFe_2O_4$ nanoparticles synthesized at 80 °C, revealing an inverse spinel structure.

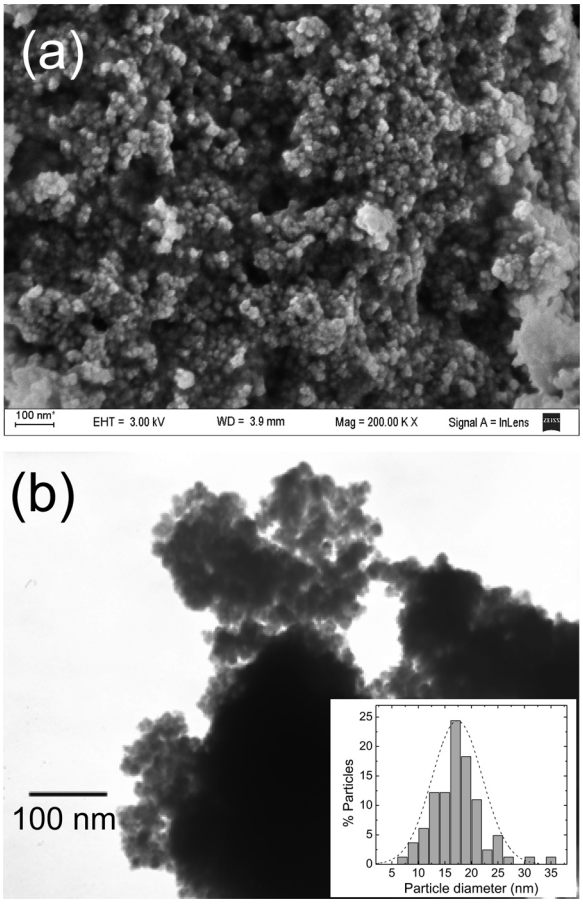

Fig. 2. (a) Scanning electron microscopy image of $CoFe_2O_4$ nanoparticles as obtained; (b) transmission electron microscopy image of these particles; inset: particle size histogram.

$$d_c \approx \frac{9\sqrt{AK}}{\mu_0 M_S^2} \quad (2)$$

where A is the exchange stiffness constant, K the anisotropy constant, μ_0 the vacuum permittivity and M_S the saturation magnetization. Using bulk $CoFe_2O_4$ parameters reported by Hu et al. [47] a value of $d_C \approx 79$ nm is found; experimental results [48] allow to estimate it as about 60–70 nm.

3.2. $CoFe_2O_4$–PANI composites characterization

3.2.1. Thermal stability and composition

To study the thermal stability of the resulting composites and to gain insight into their composition, thermogravimetric (TG) analysis in air was conducted (Fig. 3); it is observed that PANI is completely decomposed by oxidation and the ferrite particles undergo only a small mass loss, whereas the composites give intermediate results, thus, confirming the composite formation. The features in Fig. 3 can be explained as follows: first, an initial mass loss is observed, attributable to removal of water from the material; this loss ends at about 150 °C, and from this temperature, the dopant (HCl) is removed [49–51]. At higher temperature, T, a pronounced decrease is observed, corresponding to PANI decomposition, starting between 250–300 °C and ending at ~600 °C; this is in agreement with literature reports, where PANI degradation in the range ~200–660 °C is observed [51,52]. The onset of polymer degradation has been found to lie at different values, from about 180 °C [53] to nearly 300 °C [51]; in the present experiments, analysis of the TG derivatives show a change of behavior at 263 °C,

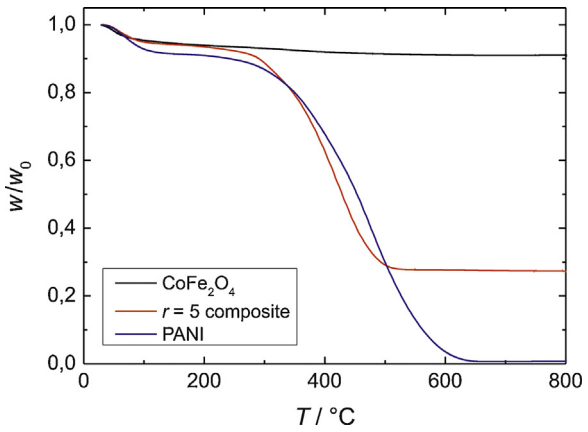

Fig. 3. Thermograms of the relative mass loss (w/w_0) for pure cobalt ferrite and PANI and for the composite with a monomer: ferrite molar ratio $r = 5$.

thus, this value is taken as the start of PANI decomposition. On the other hand, pure ferrite particles show, after some water elimination, a small decrease probably due to loss of surface hydroxyl groups. From the TG results, both the dopant contents and the composites composition can be estimated, assuming that the mass loss at $T < 150\,^{\circ}C$ is due to water elimination, that the loss between 150 and 263 °C corresponds to HCl removal, and the remaining mass at $T = 800\,^{\circ}C$ corresponds to the ferrite particles with no polymer remaining, introducing appropriate corrections for the mass change of the cobalt ferrite particles. The results for the $CoFe_2O_4$ mass fraction in the composite, f_{CF}, the measured polymer/ferrite molar ratio, r_m, and the HCl/monomoer molar ratio, y, are presented in Table 1. An apparent increase of polymer contents comparing with the synthesis bath composition is observed, which is attributable to the reduction of the particle size during the composite preparation. The y values indicate a low level of doping, corresponding to about 1 HCl molecule for about 11–15 aniline monomer units.

3.2.2. Composite morphology

The morphology of the composites was examined in SEM and TEM images. For comparison, Fig. 4 shows SEM images of PANI synthesized in the same conditions as the composites. At low magnification (2K×), the polymer appears with a rather compact surface; however, at higher magnifications, the presence of nanofibers is revealed, and at the higher magnification shown (200K×) the nanofiber tips are observed. From the TEM images of the composites (Fig. 5), the particle size in the composites d_{PC} was determined with the same method as the bare particles, ranging between (11.9 ± 1.9) nm and (13.7 ± 2.6) nm, which is somewhat smaller than the original size, but is found to be nearly independent of the ratio r and is still within the ferromagnetic monodomain size range. The images suggest that some particle agglomeration is present in the composites, despite the strong stirring during the synthesis; this is clearly due to their strong magnetic nature, and the same is observed in literature reports of similar materials [23,24,35,54]; it should be noted, however, that darker parts of the composites correspond to thicker polymer segments, thus, the apparent agglomeration observed in these regions is partly due to the presence of nanoparticles at different heights, appearing as aggregates in the vertical TEM observation.

Fig. 5a shows that the composite with $r = 5$ has a globular morphology, presenting spheres of about 65 nm diameter, some of which contain ferrite nanoparticles; this morphology is at difference with pure PANI, which in the same synthesis conditions presents a fibrous structure (Fig. 4). For $r = 10$, Fig. 5c and d, the polymer morphology is more compact and homogeneous, with the particles dispersed more uniformly. Finally, for $r = 20$, Fig. 5e and f, the fibrous morphology of pure PANI is recovered, with the ferrite particles more dispersed, as expected. These changes can be attributed to the change in the monomer:ferrite ratio, compared with pure PANI, thus, lower r leads to a more globular morphology. This can be explained by a nucleation effect of the particles, because Ani is allowed to adsorb prior to polymerization: low r results in a relatively large number of nuclei where Ani polymerizes and is rapidly consumed, thus, growing is limited and a globular morphology is obtained; with fewer particles for the same amount of monomer growing is larger and the globular morphology is lost.

3.2.3. Electrical conductivity

The electrical conductivity of PANI and the composites as-obtained here resulted quite low, ranging from $2.8 \times 10^{-6}\,S\,cm^{-1}$ for PANI–PVP to $1.3 \times 10^{-8}\,S\,cm^{-1}$ for the composite with $r_m = 5.9$ (30% w/w ferrite), with a monotonous decrease as the ferrite contents increases. These results are collected in Table 2, compared with the polymer:ferrite measured molar ratio, r_m, and the cobalt ferrite mass fraction f_{CF}. These low values can be attributed, at least in part, to the low doping level found in the TG measurements; for redoped composites, the conductivities were about 1–2 orders of magnitude higher, ranging from $2.1 \times 10^{-5}\,S\,cm^{-1}$ for PANI–PVP to $1.1 \times 10^{-6}\,S\,cm^{-1}$ for $r = 5$, indicating that the composites became dedoped during the washing and purification procedure, but that redoping did not restore the expected PANI conductivity, possibly due to a compact structure resulting after drying. These low conductivity values, besides low doping level, can be attributed to the synthesis conditions: the low Ani concentration leads to short polymer chains and low conductivity, as reported by Rakić et al. [55]. Nevertheless, the conductivity decreases with increasing ferrite contents, as expected [21].

3.2.4. IR spectroscopy

IR spectroscopy gives confirmation of the presence of the diverse components and provides information about their interactions. We will consider here the region between 400–$1800\,cm^{-1}$, which is shown in Fig. 6. From bottom up, the spectra of the separate composite components, namely PANI, PVP and $CoFe_2O_4$, are shown. The IR response of PANI has been studied by many authors [56–58]; here we will concentrate on some important bands which are marked by dashed vertical lines: the bands at 1589 and $1501\,cm^{-1}$ (ring deformation vibrations), the $1300\,cm^{-1}$ C—N stretching band; the band at $1147\,cm^{-1}$ (attributed to ring-N vibrations [59]), another band at $828\,cm^{-1}$ (out of plane C—H), and finally that at $506\,cm^{-1}$ (ring deformation mode). The following spectrum, in Fig. 6b, corresponds to PVP; its IR behavior

Table 1
Composites composition found by thermogravimetric analysis.

Synthesis composition, r	Measured composition, r_m	Fe_2CoO_4 mass fraction, f_{CF}	HCl/monomer molar ratio, y
PANI	-	0	0.06
5	5.9	0.30	0.08
10	20.8	0.11	0.08
20	24.1	0.095	0.09

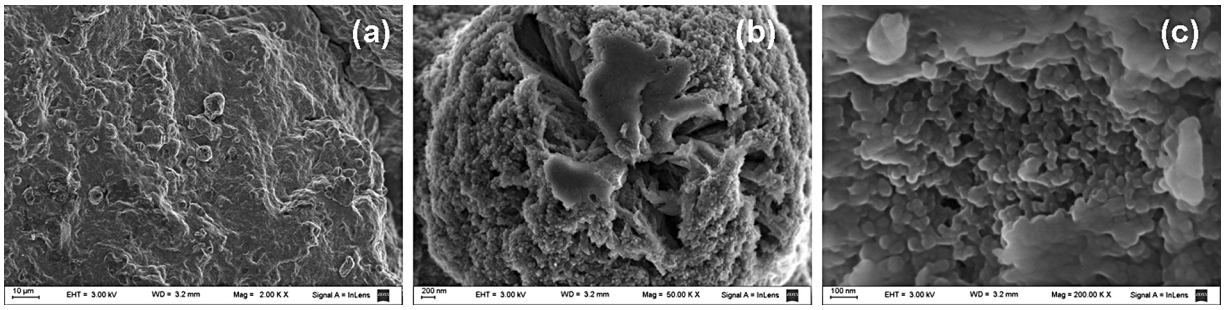

Fig. 4. SEM images of poly(aniline) obtained in the same conditions as the composites at different magnifications: (a) 2K×, (b) 50K× and (c) 200K×.

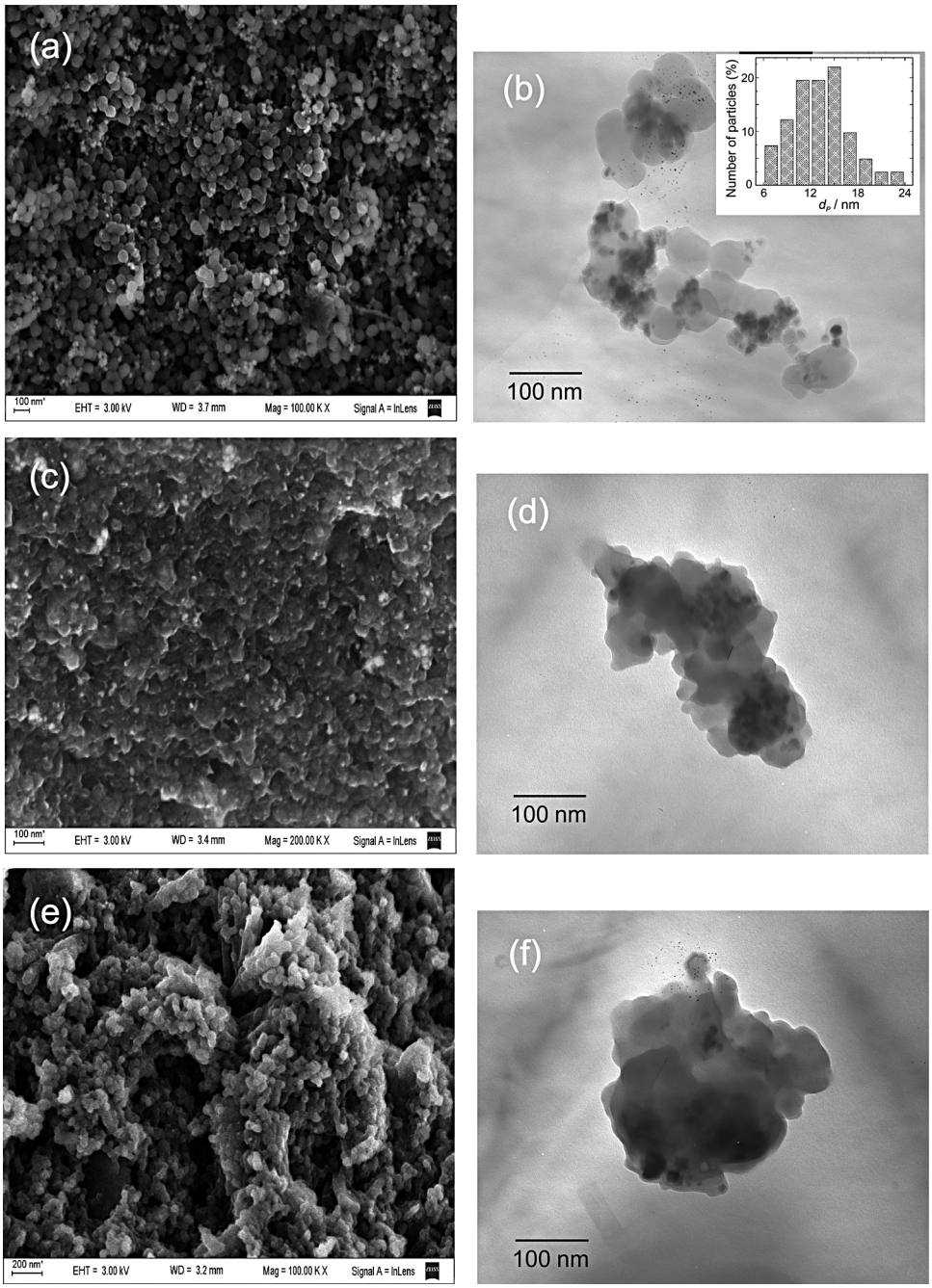

Fig. 5. Electron microscopy images of $CoFe_2O_4$–PANI composites; (a), (c) and (e), SEM images; (b), (d) and (f), TEM images (a), (b) $r = 5$; (c), (d), $r = 10$; (e), (f) $r = 20$.

Table 2
Conductivities of pure PANI and composites.

Molar composition, r_m	$CoFe_2O_4$ mass fraction, f_{CF}	σ/S cm^{-1}
5.9	0.30	1.31×10^{-8}
20.8	0.11	2.53×10^{-8}
24.1	0.095	8.71×10^{-7}
Pure PANI		2.78×10^{-6}

has been described [60], we will note here the intense C=O stretching band at 1658 cm^{-1}, signaled by a vertical dotted line. Finally, the most intense lattice band of $CoFe_2O_4$ (Fig. 6c) lies at 588 cm^{-1}, being indicated by a dash-dotted line. Fig. 6d shows the spectrum of PANI synthesized in the presence of PVP. Starting from the high wavenumber end, the PVP C=O band is detected, thus, confirming its presence in the product; next, some PANI bands show some changes: the band originally at 1589 cm^{-1} in the ring stretching region show a displacement to lower energies, also suggesting some splitting; the band at 1300 cm^{-1} is displaced to lower wavenumbers, and finally that at 1147 cm^{-1} shows a decrease in intensity and a noticeable splitting; these findings indicate an interaction between the two polymers, possibly through hydrogen bonding between NH groups of PANI and N and or O atoms of the PVP. Fig. 6e shows the spectrum of the PANI–$CoFe_2O_4$ composite obtained without PVP where it is observed the presence of the 588 cm^{-1} ferrite band; neither this band nor those of PANI appear noticeably affected, except for a small decrease of the 506 cm^{-1} PANI band; these observations indicate that the PANI–ferrite interactions are less intense than for the PANI–PVP case. At the top of Fig. 6, the full composite spectrum (for $r = 10$) is presented; the PVP band at 1658 cm^{-1} is again observed, confirming its presence in the composite material. The PANI bands show changes similar to the PANI–PVP case (Fig. 6d), indicating interaction between the two polymers, and the $CoFe_2O_4$ band at 588 cm^{-1} also appears displaced to lower energies, indicating interactions between ferrite and PVP and/or PANI. Thus, the IR results support the composite structure formed by cobalt ferrite particles covered with a PVP layer and embedded in PANI, as expected from the preparation procedure.

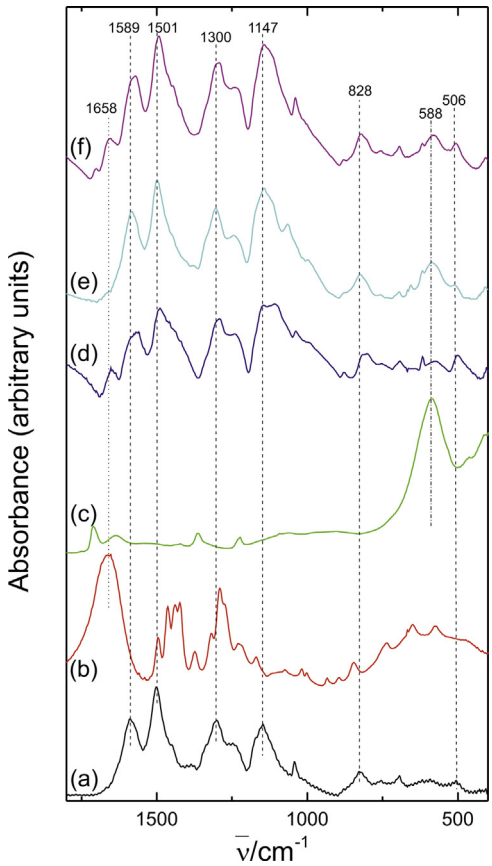

Fig. 6. IR spectra for the 400–1800 cm^{-1} region of (a) pure PANI; (b) poly (vinylpyrrolidone) (PVP); (c) $CoFe_2O_4$ particles; (d) PANI synthesized in the presence of PVP (PANI–PVP); (e) composite with $r = 5$ without PVP; (f) composite with $r = 10$. The vertical dotted line indicates the position of the C=O stretching band in pure PVP; the vertical dashed lines indicate band positions of pure PANI, and the dash-dotted line at right indicates the position of the main cobalt ferrite band.

Some features of the PANI spectrum are dependent on the doping level. As stated by several authors [61–65], the location of the ring deformation bands (1501 and 1589 cm^{-1}) and the ring-N band at 1147 cm^{-1} are affected by protonation. As remarked by Kulszewicz-Bajer et al. [63], the ring-N band is a good indicator of the doping state, shifting from 1160 to 1130 cm^{-1} in going from the undoped base to the fully doped salt forms, with most of the change taking place in the initial steps of the doping process; a similar range is reported by other authors [61,65]. In Fig. 6a, this band is located at 1147 cm^{-1}, indicating a low level of doping, in agreement with the TG results; in Ref. [63], this band shifted from 1160 to about 1137 cm^{-1} when y changed from 0 to 0.03; because the different dopant employed (poly(hexamethylene phosphate)), the results cannot be compared directly with the present ones, but are similarly low, thus, they can be seen as consistent. The position of the ring deformation bands also undergo red shifts upon doping, but in this case, different authors report slightly different ranges, as shown in Table 3. In general, it is observed that the present results fall at, or near the base forms; for example, considering the recent review of Trchová et al. [65], the lower energy band position is coincident with the reported wavenumber for the base form, whereas the upper energy band location falls between both forms, but closer to the undoped one. Thus, the IR results indicate a low level of doping, which is consistent with the TG and conductivity results.

3.3. Magnetization behavior

3.3.1. Magnetization results

Fig. 7 shows the mass magnetization, M, as a function of the magnetic field H for the bare particles and several composites. The magnetization is referred to the composite mass, thus, the curves have smaller M values as the contents of magnetic particles decreases. The curve for the bare particles is similar to others reported in the literature [8,14,45], showing hysteresis which reveals ferromagnetic behavior. The curves for the composites show a similar behavior, indicating that the particles essentially keep their ferromagnetic nature, as it has been reported for similar composites; at the extremes of the H range (±10 kOe), the curve corresponding to the bare particles ($r = 0$) reaches a value $M_{max} = 54.1$ emu g^{-1}, somewhat lower than the saturation magnetization reported for cobalt ferrite particles of about 70 emu g^{-1} [8,14]. It should be noted that at $H = 10$ kOe there is a noticeable slope in the curve, thus, M_S should be somewhat higher; this point is addressed below.

In order to compare more closely the above curves, they are presented in Fig. 8 in the form of relative magnetization $m = M/M_{max}$. The inset shows the curves in the full range, where it is observed that all the curves merge for high field values, showing the same slope. The main graph shows an enlarged view of the low field region, revealing that the remanence M_r increases as the polymer contents increases, and also a relatively small change (in terms of the H range) in the coercivity H_c is found. These results indicate that there is a change in the magnetic properties when the

Table 3
Ring deformation bands[a].

Band	This work	Cao [58]		McCall [59]		Sariciftci [61]		Kulszewicz-Bajer [60]		Trchová [62]	
		B	S	B	S	B	S	B	S	B	S
Low ring def. (~1500)	1501	1492	1486	1501	1486	1510	1491	1493	1479	1501	1477
High ring def. (~1600)	1589	1586	1563	1591	1568	1599	1580	1583	1571	1591	1561

B and S indicate base and salt forms, respectively.
[a] Wavenumbers in cm^{-1}.

particles are included in the composite; otherwise, if a simple "dilution" effect was taking place, all the normalized curves should be coincident. The nearly constancy of H_c can in principle be interpreted observing that the particles are, as discussed above, magnetic monodomains, and in this case H_c is a function of particle size [4]. Albeit an increase in coercivity could in principle lead to an improvement in microwave shielding efficiency, it is found by several authors that the nature and concentration of magnetic nanoparticles are the relevant parameters controlling shielding efficiency [23,34,51].

Comparing the normal composite with the no-PVP case (Fig. 9) the relative magnetization curves shows a very good coincidence, revealing that the presence of PVP does not affect the magnetic behavior of the ferrite particles; the slight difference in size does not alter significantly the magnetic properties, either.

3.3.2. Analysis of magnetization curves

The most important feature found is the dependence of the relative remanence and coercivity on the amount of polymer present, which is not expected from a simple dilution effect of the magnetic material, which would result in an exact overlay of all the normalized curves. To further analyze these results, the magnetization curves are interpreted as the superposition of ferromagnetic and superparamagnetic contributions. This is based on the fact that the surface layer of magnetic particles is magnetically disordered due to several factors such as atom vacancies and loss of spin exchange coupling between iron atoms, resulting in effects such as spin canting [1,66,67]; also interactions between the ferrite surface and the polymer matrix could affect the magnetic properties of the surface layer. Thus, the magnetization is assumed to obey the following expression [68]:

$$M(H) = \frac{2M_F}{\pi}\arctan\left[\frac{H \pm H_c}{H_c}\tan\left(\frac{\pi M_r}{2M_F}\right)\right] + M_{SP}\left[\coth\left(\frac{\mu H}{kT}\right) - \frac{kT}{\mu H}\right] \quad (3)$$

where M_F and M_{SP} are the saturation values of the ferromagnetic and superparamagnetic parts, respectively, μ is the average magnetic moment of the superparamagnetic contribution per particle and k and T have their usual meanings. Additionally, the overall saturation magnetization is $M_S = M_F + M_{SP}$. The first term in Eq. (3) is the usual function used to represent a ferromagnetic hysteresis curve, whereas the second term is the well known Langevin function. The relative magnetization m is thus given by

$$m(H) = \frac{M(H)}{M_{max}} = \frac{2m_F}{\pi}\arctan\left[\frac{H \pm H_c}{H_c}\tan\left(\frac{\pi m_r m_S}{2m_F}\right)\right] + (m_S - m_F)\left[\coth\left(\frac{\mu H}{kT}\right) - \frac{kT}{\mu H}\right] \quad (4)$$

where $m_F = M_F/M_{max}$, $m_r = M_r/M_S$ is the remanence ratio and $m_S = M_S/M_{max}$; as it was observed in Fig. 8, M_{max} cannot be identified with M_S, and it was found that doing so resulted in a clearly unsatisfactory fitting. Eq. (4) was fitted to the upper branch of the experimental data of Fig. 8, imposing the restriction that m_S has a common value for all curves, based on the coincidence of all the curves at high fields; it resulted $m_S = 1.089 \pm 0.004$. The fitting is very good, as it can be seen in Fig. 10. Fig. 11 shows the dependence of the remanence ratio and the coercivity with the material composition. Table 4 collects the remaining results; the absolute magnetization values are obtained using the M_{max} ones of Fig. 7. From the fitting, a value of 59 emu g^{-1} is found for M_S of the $CoFe_2O_4$ particles; albeit it is strictly an extrapolated value, it compares well with literature data [8,14,69], and is somewhat lower than the reported bulk values of 60–90 emu g^{-1} [14,70], as expected. The ratio m_F increases in going from the bare particles to the composites; it is better to convert it to the ferromagnetic fraction $f_F = M_F/M_S = m_F/m_S$, resulting $f_F = 0.69$ for the bare particles and $f_F = 0.83$ for the composites.

The most interesting feature is the dependence of m_r and H_c with composition, r_m, shown in Fig. 11. The dependence of the

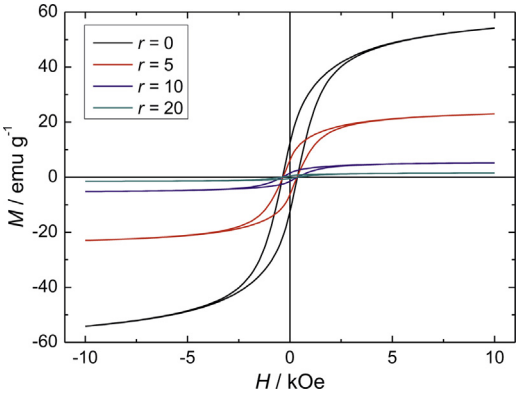

Fig. 7. Magnetization curves at 298 K for the $CoFe_2O_4$ particles and composites with the indicated compositions. 1 emu g^{-1} = 1 A m^2 kg^{-1}; 1 Oe = $10^3(4\pi)^{-1}$ A m^{-1}.

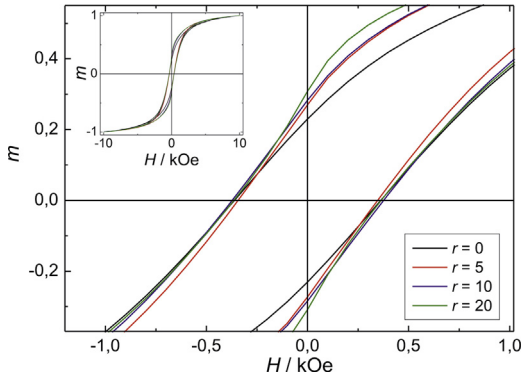

Fig. 8. Normalized magnetization curves for cobalt ferrite particles and composites. The inset shows the full curves whereas the main plot shows an enlarged view of the region close to the origin.

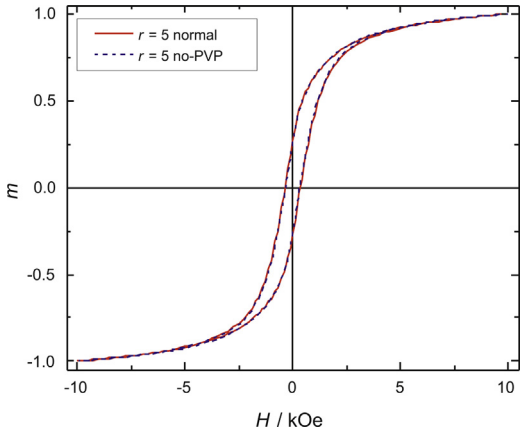

Fig. 9. Comparison of the magnetization curves for $r = 5$ with and without PVP covering the ferrite particles. The curves are almost identical.

remanence ratio on r_m indicates an increase of remanent magnetization as the polymer contents increases for a fixed amount of ferrite. The values of H_c are low comparing with most literature data for similar size $CoFe_2O_4$ particles [71,72]; however, the results of Maaz et al. [69] and Gajbhiye [48] for $d_P \sim 13$ nm give H_c near 400 Oe, fairly coincident with the present results; these are presumably related to a relatively low anisotropy energy. The decrease of H_c going from $r_m = 0$ to 5.9 should be due to the decrease in particle size; as reported previously [14], for nanoparticles in the monodomain regime, the coercivity decreases as the size decreases, as it has also been reported in the literature [4]. For higher r_m values, H_c qualitatively follows the increase in m_r; this is attributed to changes in the anisotropy energy with polymer contents. Recalling the reasons given above, surface effects should be discarded because they would not be dependent on the amount of PANI present in the composite; instead, they would be due, if present, to an organic layer (PVP in this case) adsorbed on the surface, independently of the total amount of polymer in the material. It is also worth noting that, for $r_m = 5.9$, the mass fraction of cobalt ferrite is $f_{CF} = 0.30$ (Table 1), thus, it should be expected that the composite would have $M_S(r = 5) = f_{CF} \times M_S(r = 0) \approx 18$ emu g^{-1}.

However, a higher value (25.0 emu g^{-1}, Table 4) is observed, thus, a contribution due to the polymer matrix is found. It is concluded that interactions between the polymer matrix and the magnetic nanoparticles causes the enhancements of coercivity and remanence ratio observed. Dipolar and exchange interactions are the most important forms [73], both capable of causing

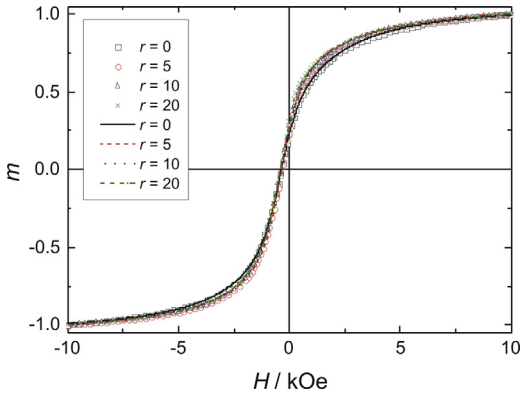

Fig. 10. Fitting of the experimental data for composites to Eq. (4).

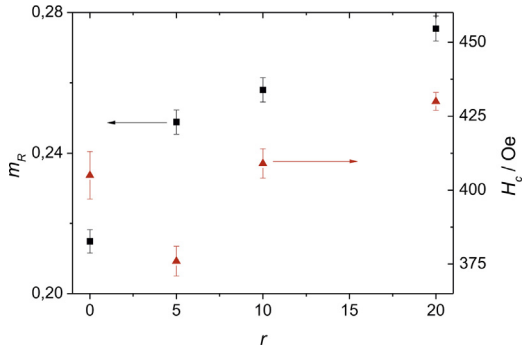

Fig. 11. Remanence ratio m_r and coercivity H_c as a function of monomer:ferrite measured ratio, from fitting to Eq. (4).

ferromagnetic behavior for nanoparticles which isolated would display superparamagnetic response; in the results presented here, the bare particles are not isolated but grouped together and agglomerated, as it is observed in Fig. 2; thus, the partial agglomeration found in the composites (Fig. 5) should not lead to increased hysteresis over the bare particles, but to the same or lower effect (equal or lower H_C and m_r), consequently these types of interaction should not explain the results of Fig. 11.

Another form of interaction is an RKKY (Ruderman–Kittel–Kasuya–Yosida) [74] mechanism, where d electrons on different lattice atoms undergo indirect exchange coupling through conducting electrons, which has been observed in magnetic nanocomposites [73]. It is a well known fact that in the conducting (doped emeraldine) form of PANI, there are highly mobile conduction electrons as well as localized paramagnetic spin states, as it has been observed by EPR [75], magnetic susceptibility [76], temperature-dependent conductivity [77] and temperature-dependent broadband spectroscopy [78] studies. Here, we propose that the isolated paramagnetic states in PANI are indirectly exchange coupled to the ferrite particles through the free conduction electrons. In the RKKY theory, the exchange Hamiltonian between two isolated spins S_i and S_j at a distance x is [46,74]

$$H(x) = S_i \times S_j \Gamma_J F(2k_F x) \tag{5}$$

where Γ_J is a coupling parameter, k_F is the Fermi wave vector, $k_F = (3\pi^2 n)^{1/3}$, n the density of free carriers and $F(y)$ is

$$F(y) = \frac{y\cos y - y\sin y}{y^4} \tag{6}$$

F is a damped oscillating function whose first zero lies at $y_0 = 2k_F x_0 = 4.49$; for y below this value the exchange is stronger and ferromagnetic [74]. Here, S_i is the nanoparticle spin and S_j is a PANI localized spin at a distance x from the particle surface. For fully doped PANI, the carrier density can be estimated to be $n \cong 4 \times 10^{27}\,m^{-3}$ [78]; in the composites synthesized here, the conductivity was found to be about 7–8 orders of magnitude lower than fully doped PANI, thus, the density of charge carriers should be considerably lower than the above value; Chen et al. [79] presented an empirical relationship between carrier density and conductivity for HCl doped PANI:

$$\log\left(\frac{\sigma}{S\ cm^{-1}}\right) = 2.954 \log\left(\frac{n}{cm^{-3}}\right) - 62.662 \tag{7}$$

According to Eq. (7), for $\sigma \approx 10^{-8}\,S\,cm^{-1}$, n is estimated as $\sim 3.2 \times 10^{24}\,m^{-3}$, $k_F \approx 4.6 \times 10^8\,m^{-1}$, thus the distance to the first zero x_0 is about 10 nm. This result suggests that a layer of polymer of ~10 nm thick is contributing to the magnetic response of the composite. The particle–particle average distance, $d_{P\text{–}P}$, can be

Table 4
Magnetization curve parameters from fitting to Eq. (4).

r_m	m_F	M_S/emu g^{-1} [a]	M_r/emu g^{-1}	M_F/emu g^{-1}	M_{SP}/emu g^{-1}	$\mu/10^{-17}$ emu
0	0.75 ± 0.02	59.0 ± 0.3	12.7 ± 0.2	41 ± 1	18 ± 1	2.4 ± 0.1
5.9	0.88 ± 0.02	25.0 ± 0.2	6.2 ± 0.1	20.2 ± 0.5	4.8 ± 0.5	1.8 ± 0.1
20.8	0.90 ± 0.02	5.7 ± 0.1	1.47 ± 0.04	4.7 ± 0.2	1.0 ± 0.1	1.7 ± 0.1
24.1	0.91 ± 0.02	1.6 ± 0.1	0.45 ± 0.03	1.4 ± 0.1	0.27 ± 0.05	1.6 ± 0.1

[a] 1 emu g^{-1} = 1 A m^2 kg^{-1}.

estimated from the mass composition found in TG experiments, assuming for simplicity a cubic arrangement (Fig. 12), and setting the cube volume to the particle volume, V, times the ratio of composite to oxide volume, resulting in:

$$d_{P-P} \approx \sqrt[3]{\frac{f_{CF}/\rho_{CF} + (1 - f_{CF})\rho_{PA}}{f_{CF}/\rho_{CF}} V} \quad (8)$$

where $\rho_{CF} = 5.29\,g\,cm^{-3}$ and $\rho_{PA} = 1.33\,g\,cm^{-3}$ are the densities of cobalt ferrite and polyaniline, respectively. For $r_m = 5.9$, 20.8 and 24.1, d_{P-P} values of 15, 20 and 23 nm, respectively, are found; these values are comparable to the estimated x_0. The increase of remanence ratio and coercivity with polymer contents can in principle be explained as follows: for low r values, x_0 is less than the distance between particle surfaces (equal to $d - 2r_P$), thus, as r increases, the amount of polymer, within a distance shorter than x_0, per particle increases, and consequently the amount of PANI localized spins interacting with each particle also increases leading to higher exchange energy, coercivity and remanence. Thus, it is proposed that RKKY-like coupling of isolated PANI spins with the magnetic nanoparticles mediated by the polymer conduction electrons is responsible for the enhancement of coercivity and remanence ratio observed.

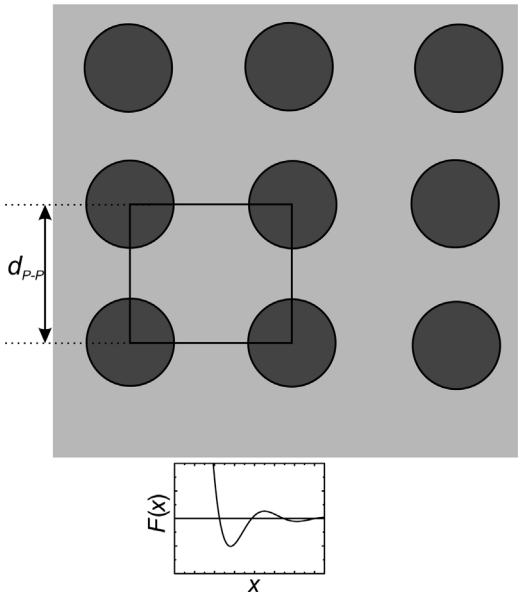

Fig. 12. Schematic representation to estimate the particle-particle average distance, d_{P-P}. Assuming for simplicity a cubic lattice, the cubic cell volume is estimated from the particle volume times the ratio of composite to particle volumes. The bottom plot is the RKKY function, $F(x)$, Eq. (6).

4. Conclusions

Cobalt ferrite–poly(aniline) composites have been synthesized in acid media. The DC magnetization measurements shows that the remanence ratio increases as the polymer contents increases, the coercivity decreases first and then increases, and the saturation magnetization does not follow the ferrite mass fraction in the composite. These results are not expected, and cannot be explained by a dilution effect of the ferromagnetic particles; instead, they indicate the presence of particle–matrix interactions, suggesting that the magnetic behavior of the $CoFe_2O_4$–poly(aniline) composite can be modulated by varying the conducting polymer content. It is proposed that RKKY-like coupling of isolated PANI spins with the magnetic nanoparticles mediated by the polymer conduction electrons is responsible for the observed magnetic behavior.

Acknowledgment

The authors gratefully acknowledge funding from the Universidad de Buenos Aires, the Consejo Nacional de Investigaciones Científicas y Técnicas (CONICET) and the Agencia Nacional de Promoción Científica y Tecnológica, all of Argentina. P. S. A., G. J. and F. V. M. are members of the Carrera del Investigador Científico of CONICET.

References

[1] R.H. Kodama, Magnetic nanoparticles, J. Magn. Magn. Mater. 200 (1999) 359–372.
[2] S.R. Chowdhury, E.K. Yanful, Arsenic and chromium removal by mixed magnetite–maghemite nanoparticles and the effect of phosphate on removal, J. Environ. Manage. 91 (2010) 2238–2247, doi:http://dx.doi.org/10.1016/j.jenvman.2010.06.003.
[3] J.S. Beveridge, J.R. Stephens, M.E. Williams, The use of magnetic nanoparticles in analytical chemistry, Annu. Rev. Anal. Chem. 4 (2011) 251–273, doi:http://dx.doi.org/10.1146/annurev-anchem-061010–114041.
[4] D.L. Leslie-Pelecky, R.D. Rieke, Magnetic properties of nanostructured materials, Chem. Mater. 8 (1996) 1770–1783, doi:http://dx.doi.org/10.1021/cm960077f.
[5] J.L. Dormann, D., Fiorani, E. Tronc, Magnetic relaxation in fine-particle systems, in: I. Prigogine, S.A. Rice (Eds.), Adv. Chem. Phys., John Wiley & Sons, Inc., New York, 2007, vol. 98, pp. 283–494. http://onlinelibrary.wiley.com/doi/10.1002/9780470141571ch4/summary (accessed 10.08.12).
[6] J. Jin, K. Hashimoto, S. Ohkoshi, Formation of spherical and rod-shaped ε-Fe_2O_3 nanocrystals with a large coercive field, J. Mater. Chem. 15 (2005) 1067, doi:http://dx.doi.org/10.1039/b416554c.
[7] A. Tavakoli, M. Sohrabi, A. Kargari, A review of methods for synthesis of nanostructured metals with emphasis on iron compounds, Chem. Pap. 61 (2007) 151–170, doi:http://dx.doi.org/10.2478/s11696-007-0014-7.
[8] Y.I. Kim, D. Kim, C.S. Lee, Synthesis and characterization of $CoFe_2O_4$ magnetic nanoparticles prepared by temperature-controlled coprecipitation method, Physica B Condens. Matter 337 (2003) 42–51, doi:http://dx.doi.org/10.1016/S0921-4526(03)00322-3.
[9] G. Mu, X. Pan, N. Chen, K. Gan, M. Gu, Preparation and magnetic properties of barium hexaferrite nanorods, Mater. Res. Bull. 43 (2008) 1369–1375, doi:http://dx.doi.org/10.1016/j.materresbull.2007.06.052.
[10] B. Leven, G. Dumpich, Resistance behavior and magnetization reversal analysis of individual Co nanowires, Phys. Rev. B 71 (2005) 64411, doi:http://dx.doi.org/10.1103/PhysRevB.71.064411.
[11] H. Chen, D. Tang, B. Zhang, B. Liu, Y. Cui, G. Chen, Electrochemical immunosensor for carcinoembryonic antigen based on nanosilver-coated

magnetic beads and gold–graphene nanolabels, Talanta 91 (2012) 95–102, doi:http://dx.doi.org/10.1016/j.talanta.2012.01.025.
[12] E. Mazarío, P. Herrasti, M.P. Morales, N. Menéndez, Synthesis and characterization of $CoFe_2O_4$ ferrite nanoparticles obtained by an electrochemical method, Nanotechnology 23 (2012) 355708, doi:http://dx.doi.org/10.1088/0957-4484/23/35/355708.
[13] S. Shin, J. Jang, Thiol containing polymer encapsulated magnetic nanoparticles as reusable and efficiently separable adsorbent for heavy metal ions, Chem. Commun. (2007) 4230, doi:http://dx.doi.org/10.1039/b707706h.
[14] P.S. Antonel, G. Jorge, O.E. Perez, A. Butera, A.G. Leyva, R.M. Negri, Magnetic and elastic properties of $CoFe_2O_4$-polydimethylsiloxane magnetically oriented elastomer nanocomposites, J. Appl. Phys. 110 (2011) 43920–43920-8, doi:http://dx.doi.org/10.1063/1.3624602.
[15] P. Chandrasekhar, Conducting Polymers, Fundamentals and Applications: A Practical Approach, first ed., Springer, New York, 1999.
[16] L. Lizarraga, E.M. Andrade, F.V. Molina, Swelling and volume changes of polyaniline upon redox switching, J. Electroanal. Chem. 561 (2004) 127–135, doi:http://dx.doi.org/10.1016/j.jelechem.2003.07.026.
[17] P.S. Antonel, E. Völker, F.V. Molina, Photophysics of polyaniline: sequence-length distribution dependence of photoluminescence quenching as studied by fluorescence measurements and Monte Carlo simulations, Polymer 53 (2012) 2619–2627, doi:http://dx.doi.org/10.1016/j.polymer.2012.04.041.
[18] Z. Guo, K. Shin, A.B. Karki, D.P. Young, R.B. Kaner, H.T. Hahn, Fabrication and characterization of iron oxide nanoparticles filled polypyrrole nanocomposites, J. Nanopart. Res. 11 (2009) 1441–1452, doi:http://dx.doi.org/10.1007/s11051–008-9531–8.
[19] C.S. Priya, G. Velraj, Synthesis and characterization of nano and micro copper doped conducting polymer, Mater. Lett. 77 (2012) 29–31, doi:http://dx.doi.org/10.1016/j.matlet.2012.02.112.
[20] K. Singh, A. Ohlan, P. Saini, S.K. Dhawan, Poly (3,4-ethylenedioxythiophene) γ-Fe_2O_3 polymer composite–super paramagnetic behavior and variable range hopping 1D conduction mechanism–synthesis and characterization, Polym. Adv. Technol. 19 (2008) 229–236, doi:http://dx.doi.org/10.1002/pat.1003.
[21] P. Dallas, N. Moutis, E. Devlin, D. Niarchos, D. Petridis, Characterization, electrical and magnetic properties of polyaniline/maghemite nanocomposites, Nanotechnology 17 (2006) 5019–5026, doi:http://dx.doi.org/10.1088/0957-4484/17/19/041.
[22] Y.-J. Zhang, Y.-W. Lin, C.-C. Chang, T.-M. Wu, Conducting and magnetic behaviors of polyaniline coated multi-walled carbon nanotube composites containing monodispersed magnetite nanoparticles, Synth. Met. 161 (2011) 937–942, doi:http://dx.doi.org/10.1016/j.synthmet.2011.02.026.
[23] N. Gandhi, K. Singh, A. Ohlan, D.P. Singh, S.K. Dhawan, Thermal, dielectric and microwave absorption properties of polyaniline–$CoFe_2O_4$ nanocomposites, Compos. Sci. Technol. 71 (2011) 1754–1760, doi:http://dx.doi.org/10.1016/j.compscitech.2011.08.010.
[24] X. Zhang, S. Wei, N. Haldolaarachchige, H.A. Colorado, Z. Luo, D.P. Young, et al., Magnetoresistive conductive polyaniline–barium titanate nanocomposites with negative permittivity, J. Phys. Chem. C 116 (2012) 15731–15740, doi:http://dx.doi.org/10.1021/jp303226u.
[25] H. Gu, Y. Huang, X. Zhang, Q. Wang, J. Zhu, L. Shao, et al., Magnetoresistive polyaniline-magnetite nanocomposites with negative dielectrical properties, Polymer 53 (2012) 801–809, doi:http://dx.doi.org/10.1016/j.polymer.2011.12.033.
[26] H. Gu, S. Tadakamalla, Y. Huang, H.A. Colorado, Z. Luo, N. Haldolaarachchige, et al., Polyaniline stabilized magnetite nanoparticle reinforced epoxy nanocomposites, ACS Appl. Mater. Interfaces. 4 (2012) 5613–5624, doi:http://dx.doi.org/10.1021/am301529t.
[27] X. Zhang, J. Zhu, N. Haldolaarachchige, J. Ryu, D.P. Young, S. Wei, et al., Synthetic process engineered polyaniline nanostructures with tunable morphology and physical properties, Polymer 53 (2012) 2109–2120, doi:http://dx.doi.org/10.1016/j.polymer.2012.02.042.
[28] J. Zhu, H. Gu, Z. Luo, N. Haldolaarachige, D.P. Young, S. Wei, et al., Carbon nanostructure-derived polyaniline metacomposites: electrical, dielectric, and giant magnetoresistive properties, Langmuir 28 (2012) 10246–10255, doi:http://dx.doi.org/10.1021/la302031f.
[29] R. Gangopadhyay, A. De, Conducting polymer nanocomposites: a brief overview, Chem. Mater. 12 (2000) 608–622, doi:http://dx.doi.org/10.1021/cm990537f.
[30] J. Pyun, Nanocomposite materials from functional polymers and magnetic colloids, Polym. Rev. 47 (2007) 231–263, doi:http://dx.doi.org/10.1080/15583720701271294.
[31] S. Radhakrishnan, S. Prakash, C.R.K. Rao, M. Vijayan, Organically soluble bifunctional polyaniline–magnetite composites for sensing and supercapacitor applications, Electrochem. Solid-State Lett. 12 (2009) A84, doi:http://dx.doi.org/10.1149/1.3074315.
[32] M. Bhaumik, T.Y. Leswifi, A. Maity, V.V. Srinivasu, M.S. Onyango, Removal of fluoride from aqueous solution by polypyrrole/Fe_3O_4 magnetic nanocomposite, J. Hazard. Mater. 186 (2011) 150–159, doi:http://dx.doi.org/10.1016/j.jhazmat.2010.10.098.
[33] S.C. Wuang, K.G. Neoh, E.-T. Kang, D.W. Pack, D.E. Leckband, Synthesis and functionalization of polypyrrole-Fe_3O_4 nanoparticles for applications in biomedicine, J. Mater. Chem. 17 (2007) 3354–3362, doi:http://dx.doi.org/10.1039/B702983G.
[34] Z. Wang, H. Bi, J. Liu, T. Sun, X. Wu, Magnetic and microwave absorbing properties of polyaniline/γ-Fe_2O_3 nanocomposite, J. Magn. Magn. Mater. 320 (2008) 2132–2139, doi:http://dx.doi.org/10.1016/j.jmmm.2008.03.043.
[35] K. Singh, A. Ohlan, A.K. Bakhshi, S.K. Dhawan, Synthesis of conducting ferromagnetic nanocomposite with improved microwave absorption properties, Mater. Chem. Phys. 119 (2010) 201–207, doi:http://dx.doi.org/10.1016/j.matchemphys.2009.08.060.
[36] B. Belaabed, J.L. Wojkiewicz, S. Lamouri, N. El Kamchi, T. Lasri, Synthesis and characterization of hybrid conducting composites based on polyaniline/magnetite fillers with improved microwave absorption properties, J. Alloys Compd. 527 (2012) 137–144, doi:http://dx.doi.org/10.1016/j.jallcom.2012.02.179.
[37] J. Anand, S. Palaniappan, D. Sathyanarayana, Conducting polyaniline blends and composites, Prog. Polym. Sci. 23 (1998) 993–1018, doi:http://dx.doi.org/10.1016/S0079-6700(97)00040-3.
[38] G.D. Prasanna, H.S. Jayanna, A.R. Lamani, S. Dash, Polyaniline/$CoFe_2O_4$ nanocomposites: a novel synthesis, characterization and magnetic properties, Synth. Met. 161 (2011) 2306–2311, doi:http://dx.doi.org/10.1016/j.synthmet.2011.08.039.
[39] A. Chen, H. Wang, B. Zhao, X. Li, The preparation of polypyrrole–Fe_3O_4 nanocomposites by the use of common ion effect, Synth. Met. 139 (2003) 411–415, doi:http://dx.doi.org/10.1016/S0379-6779(03)00190-5.
[40] P. Montoya, F. Jaramillo, J. Calderón, S.I. Córdoba de Torresi, R.M. Torresi, Evidence of redox interactions between polypyrrole and Fe_3O_4 in polypyrrole–Fe_3O_4 composite films, Electrochim. Acta 55 (2010) 6116–6122, doi:http://dx.doi.org/10.1016/j.electacta.2009.09.042.
[41] J. Deng, Y. Peng, C. He, X. Long, P. Li, A.S.C. Chan, Magnetic and conducting Fe_3O_4–polypyrrole nanoparticles with core–shell structure, Polym. Int. 52 (2003) 1182–1187, doi:http://dx.doi.org/10.1002/pi.1237.
[42] S. Xuan, Y.-X.J. Wang, J.C. Yu, K.C.-F. Leung, Preparation, characterization, and catalytic activity of core/shell Fe_3O_4@polyaniline@Au nanocomposites, Langmuir 25 (2009) 11835–11843, doi:http://dx.doi.org/10.1021/la901462t.
[43] S. Sun, H. Zeng, D.B. Robinson, S. Raoux, P.M. Rice, S.X. Wang, et al., Monodisperse MFe_2O_4 (M = Fe, Co, Mn) nanoparticles, J. Am. Chem. Soc. 126 (2004) 273–279, doi:http://dx.doi.org/10.1021/ja0380852.
[44] W. Rasband, Image J, National Institute of Health, Research Services Branch, Bethesda, Maryland, USA, 2012.
[45] Y. Qu, H. Yang, N. Yang, Y. Fan, H. Zhu, G. Zou, The effect of reaction temperature on the particle size, structure and magnetic properties of coprecipitated $CoFe_2O_4$ nanoparticles, Mater. Lett. 60 (2006) 3548–3552, doi:http://dx.doi.org/10.1016/j.matlet.2006.03.055.
[46] R.C. O'Handley, Modern Magnetic Materials: Principles and Applications, first ed., Wiley-Interscience, New York, 1999 pp. 172 and 303.
[47] J.-M. Hu, G. Sheng, J.X. Zhang, C.W. Nan, L.Q. Chen, Phase-field simulation of strain-induced domain switching in magnetic thin films, Appl. Phys. Lett. 98 (2011) 112505–112505-3, doi:http://dx.doi.org/10.1063/1.3567542.
[48] N.S. Gajbhiye, S. Prasad, G. Blaji, Experimental study of Hopkinson effect in single domain $CoFe_2O_4$ particles, IEEE Trans. Magn. 35 (1999) 2155–2161, doi:http://dx.doi.org/10.1109/20.774187.
[49] S. Palaniappan, B.H. Narayana, Temperature effect on conducting polyaniline salts: thermal and spectral studies, J. Polym. Sci. A Polym. Chem. 32 (1994) 2431–2436, doi:http://dx.doi.org/10.1002/pola.1994.080321304.
[50] J. Prokeš, M. Trchová, D. Hlavatá, J. Stejskal, Conductivity ageing in temperature-cycled polyaniline, Polym. Degrad. Stab. 78 (2002) 393–401, doi:http://dx.doi.org/10.1016/S0141-3910(02)00193–3.
[51] M. Khairy, Synthesis, characterization, magnetic and electrical properties of polyaniline/$NiFe_2O_4$ nanocomposite, Synth. Met. 189 (2014) 34–41, doi:http://dx.doi.org/10.1016/j.synthmet.2013.12.022.
[52] S. Wang, Z. Tan, Y. Li, L. Sun, T. Zhang, Synthesis, characterization and thermal analysis of polyaniline/ZrO_2 composites, Thermochim. Acta 441 (2006) 191–194, doi:http://dx.doi.org/10.1016/j.tca.2005.05.020.
[53] A. Gök, B. Sari, M. Talu, Synthesis and characterization of conducting substituted polyanilines, Synth. Met. 142 (2004) 41–48, doi:http://dx.doi.org/10.1016/j.synthmet.2003.07.002.
[54] Y. Li, G. Chen, Q. Li, G. Qiu, X. Liu, Facile synthesis, magnetic and microwave absorption properties of Fe_3O_4/polypyrrole core/shell nanocomposite, J. Alloys Compd. 509 (2011) 4104–4107, doi:http://dx.doi.org/10.1016/j.jallcom.2010.12.100.
[55] A. Rakić, D. Bajuk-Bogdanović, M. Mojović, G. Ćirić-Marjanović, M. Milojević-Rakić, S. Mentus, et al., Oxidation of aniline in dopant-free template-free dilute reaction media, Mater. Chem. Phys. 127 (2011) 501–510, doi:http://dx.doi.org/10.1016/j.matchemphys.2011.02.047.
[56] E.M. Andrade, F.V. Molina, M.I. Florit, D. Posadas, IR response of poly(*o*-toluidine): spectral modifications upon redox state change, J. Electroanal. Chem. 419 (1996) 15–21.
[57] P.S. Antonel, E.M. Andrade, F.V. Molina, Copolymerization of aniline and *m*-chloroaniline. Chlorine addition and structure of the resulting material, React. Funct. Polym. 69 (2009) 197–205.
[58] M. Trchová, J. Stejskal, Polyaniline: the infrared spectroscopy of conducting polymer nanotubes (IUPAC Technical Report), Pure Appl. Chem. 83 (2011) 1803–1817, doi:http://dx.doi.org/10.1351/PAC-REP-10–02–01.
[59] E.T. Kang, K.G. Neoh, K.L. Tan, Polyaniline: a polymer with many interesting intrinsic redox states, Prog. Polym. Sci. 23 (1998) 277–324, doi:http://dx.doi.org/10.1016/S0079-6700(97)00030-0.
[60] L. İsrael, Ç. Güler, H. Yilmaz, S. Güler, The adsorption of polyvinylpyrrolidone on kaolinite saturated with sodium chloride, J. Colloid Interface Sci. 238 (2001) 80–84, doi:http://dx.doi.org/10.1006/jcis.2001.7465.

[61] Y. Cao, S. Li, Z. Xue, D. Guo, Spectroscopic and electrical characterization of some aniline oligomers and polyaniline, Synth. Met. 16 (1986) 305–315, doi:http://dx.doi.org/10.1016/0379-6779(86)90167-0.
[62] R.P. McCall, M.G. Roe, J.M. Ginder, T. Kusumoto, A.J. Epstein, G.E. Asturias, et al., IR absorption, photoinduced IR absorption, and photoconductivity of polyaniline, Synth. Met. 29 (1989) 433–438, doi:http://dx.doi.org/10.1016/0379-6779(89)90329-9.
[63] I. Kulszewicz-Bajer, J. Sobczak, M. Hasik, J. Pretula, Spectroscopic studies of polyaniline protonation with poly(alkylene phosphates), Polymer 37 (1996) 25–30, doi:http://dx.doi.org/10.1016/0032-3861(96)81596-5.
[64] N.S. Sariciftci, M. Bartonek, H. Kuzmany, H. Neugebauer, A. Neckel, Analysis of various doping mechanisms in polyaniline by optical, FTIR and Raman spectroscopy, Synth. Met. 29 (1989) 193–202, doi:http://dx.doi.org/10.1016/0379-6779(89)90296-8.
[65] M. Trchová, Z. Morávková, I. Šeděnková, J. Stejskal, Spectroscopy of thin polyaniline films deposited during chemical oxidation of aniline, Chem. Pap. 66 (2012) 415–445, doi:http://dx.doi.org/10.2478/s11696-012-0142-6.
[66] A.E. Berkowitz, J.A. Lahut, I.S. Jacobs, L.M. Levinson, D.W. Forester, Spin pinning at ferrite-organic interfaces, Phys. Rev. Lett. 34 (1975) 594–597, doi:http://dx.doi.org/10.1103/PhysRevLett.34.594.
[67] C. Vázquez-Vázquez, M. López-Quintela, M. Buján-Núñez, J. Rivas, Finite size and surface effects on the magnetic properties of cobalt ferrite nanoparticles, J. Nanopart. Res. 13 (2011) 1663–1676, doi:http://dx.doi.org/10.1007/s11051-010-9920-7.
[68] M.B. Stearns, Y. Cheng, Determination of para- and ferromagnetic components of magnetization and magnetoresistance of granular Co/Ag films (invited), J. Appl. Phys. 75 (1994) 6894, doi:http://dx.doi.org/10.1063/1.356773.
[69] K. Maaz, A. Mumtaz, S.K. Hasanain, A. Ceylan, Synthesis and magnetic properties of cobalt ferrite ($CoFe_2O_4$) nanoparticles prepared by wet chemical route, J. Magn. Magn. Mater. 308 (2007) 289–295, doi:http://dx.doi.org/10.1016/j.jmmm.2006.06.003.
[70] F. Bensebaa, F. Zavaliche, P. L'Ecuyer, R. Cochrane, T. Veres, Microwave synthesis and characterization of Co–ferrite nanoparticles, J. Colloid Interface Sci. 277 (2004) 104–110, doi:http://dx.doi.org/10.1016/j.jcis.2004.04.016.
[71] Q. Song, Z.J. Zhang, Shape control and associated magnetic properties of spinel cobalt ferrite nanocrystals, J. Am. Chem. Soc. 126 (2004) 6164–6168, doi:http://dx.doi.org/10.1021/ja049931r.
[72] R.M. Mohamed, M.M. Rashad, F.A. Haraz, W. Sigmund, Structure and magnetic properties of nanocrystalline cobalt ferrite powders synthesized using organic acid precursor method, J. Magn. Magn. Mater. 322 (2010) 2058–2064, doi:http://dx.doi.org/10.1016/j.jmmm.2010.01.034.
[73] S. Mørup, M.F. Hansen, C. Frandsen, Magnetic interactions between nanoparticles, Beilstein J. Nanotechnol. 1 (2010) 182–190, doi:http://dx.doi.org/10.3762/bjnano.1.22.
[74] C. Kittel, Quantum Theory of Solids, second revised edition, Wiley, New York, 1987.
[75] V.I. Krinichnyi, A.L. Konkin, A.P. Monkman, Electron paramagnetic resonance study of spin centers related to charge transport in metallic polyaniline, Synth. Met. 162 (2012) 1147–1155, doi:http://dx.doi.org/10.1016/j.synthmet.2012.04.030.
[76] P.K. Kahol, A. Raghunathan, B.J. McCormick, A magnetic susceptibility study of emeraldine base polyaniline, Synth. Met. 140 (2004) 261–267, doi:http://dx.doi.org/10.1016/S0379-6779(03)00371-0.
[77] N.T. Kemp, G.U. Fianagan, A.B. Kaiser, H.J. Trodahl, B. Chapman, A.C. Partridge, et al., Temperature-dependent conductivity of conducting polymers exposed to gases, Synth. Met. 101 (1999) 434–435, doi:http://dx.doi.org/10.1016/S0379-6779(98)01118-7.
[78] R. Pelster, G. Nimtz, B. Wessling, Fully protonated polyaniline: hopping transport on a mesoscopic scale, Phys. Rev. B 49 (1994) 12718–12723, doi:http://dx.doi.org/10.1103/PhysRevB.49.12718.
[79] X. Chen, L. Shen, C.A. Yuan, C.K.Y. Wong, G. Zhang, Molecular model for the charge carrier density dependence of conductivity of polyaniline as chemical sensing materials, Sens. Actuators B 177 (2013) 856–861, doi:http://dx.doi.org/10.1016/j.snb.2012.12.009.